



Precision direction and compact surface type representation for 3D palmprint identification

Lunke Fei^a, Bob Zhang^b, Yong Xu^{c,*}, Wei Jia^d, Jie Wen^c, Jigang Wu^a

^aSchool of Computer Science and Technology, Guangdong University of Technology, Guangzhou, China

^bDepartment of Computer and Information Science, University of Macau, Taipa, Macau, China

^cSchool of Computer Science and Technology, Harbin Institute of Technology (Shenzhen), Shenzhen, China

^dSchool of Computer and Information, Hefei University of Technology, Hefei, China

ARTICLE INFO

Article history:

Received 1 March 2018

Revised 8 August 2018

Accepted 16 October 2018

Available online 22 October 2018

Keywords:

Biometrics

3D palmprint identification

Precision direction extraction

Compact surface type

ABSTRACT

Compared with its 2D counterpart, a 3D palmprint image contains not only the 3D structure-based but also the 2D texture-based features of the palmprint. In this paper, we propose a precision direction code and compact surface type (PDCST) method for 3D palmprint representation and identification. Specifically, we propose the precision direction code (PDC) to depict the 2D texture-based features by exploiting not only the visible but also the potential direction features of the palmprint. Moreover, we use a simple yet efficient compact surface type (CST) to represent the 3D structure-based features of the palmprint. We combine the PDC and CST forming the PDCST descriptor to represent the multiple level and multiple dimensional features of 3D palmprint images. The two-phase sparse representation scheme is used to perform PDCST-based feature identification. Extensive inter-comparative and intra-comparative experimental results on three widely used palmprint databases clearly demonstrate the effectiveness of the proposed method.

© 2018 Elsevier Ltd. All rights reserved.

1. Introduction

In modern society, the ability to reliably identify individuals is one of the most critical requirements in many personal recognition applications, including civilian, commercial and forensics applications [1–4]. The conventional technologies of identifying individuals are usually based on external token-based or knowledge-based means, such as the smart card, password and PIN codes. It is known that both the token-based and the knowledge-based means can be lost, forgotten or even stolen. Biometrics, which refers to automatically recognizing individuals based on one's unique physiological and behavioral traits, can provide us an effective and efficient way for personal authentication. Up to now, biometrics has been receiving increasing research attention. Various kinds of biometrics traits have been successfully developed, such as face, fingerprint, iris, gait and speech, for recognizing individuals [1–6].

As a relatively new biometric trait, palmprint based recognition has also received considerable research attention due to its merits of high discriminability and ease of collection [7–9]. For example, palmprint contains not only the rich intrinsic principal line features but also minutiae points (e.g. ridge endings and ridge bifur-

cations). These features are deemed to be permanent and unique to an individual [10,11]. In addition, palmprint image acquisition is easily accepted by users because of its easy self-positioning. Therefore, palmprint is a promising biometric trait with the potential of providing a high accuracy and user-friendliness for personal authentication [12].

To date, a variety of efforts have been diverted into palmprint recognition [7–16]. Various palmprint recognition technologies have been developed, including low-resolution palmprint recognition and high-resolution palmprint recognition. In general, the low-resolution palmprint recognition has the ability of achieving a high accuracy in real-time, which is suitable for civilian and commercial usages [17]. Comparatively, high-resolution palmprint recognition is mainly used for forensic and law enforcement applications with high-security requirements [18].

For low-resolution palmprint recognition, Zhang et al. [17] proposed a representative palmprint verification system by using the direction features of palmprint. Since then, various methods were proposed for palmprint recognition. The original palmprint recognition methods generally focus on the intrinsic features of palmprint, such as the line based features of palmprint [11,19]. Further, the direction-based coding methods became very active in recent years and achieved very promising recognition performance [20–26]. In addition, the common image-based machine-learning

* Corresponding author

E-mail address: yongxu@ymail.com (Y. Xu).

methods can also be applied for palmprint recognition. Up to now, the subspace learning, sparse representation and deep-learning methods have been successfully used for palmprint recognition [9,27–29]. Zhang et al. [15] comparatively studied and summarized the representative methods of palmprint recognition.

Different from low-resolution palmprint images, high-resolution palmprint images generally depict the ridge-based features, including the ridge pattern and minutiae points, which are highly similar as the fingerprint. The representative high-resolution palmprint recognition methods can be found in [10,18,30]. Previous works showed us that the ridge orientation, ridge density, minutiae points and the principal lines of the palmprint are the most significant and frequently used features in high-resolution palmprint recognition. In general, the high-resolution palmprint images share similar features as well as feature extraction methods as fingerprint [10,18].

Existing palmprint recognition mainly focuses on 2D palmprint images including the low-resolution and high-resolution palmprint images. With the rapid development of 3D biometrics, 3D palmprint recognition is becoming a trend due to its several merits over the 2D counterpart [31]. For example, 3D palmprint images contain discriminative surface depth information and are hard to be counterfeited. Therefore, 3D palmprint recognition has the ability to provide robust personal authentication. The first work of 3D palmprint recognition was begun with the successful implementation of a 3D palmprint data acquisition device, with which the first 3D palmprint database was established. Since then, various methods have been proposed for 3D palmprint feature extraction and recognition. For example, Zhang et al. [32] proposed a 3D palmprint recognition method by encoding the surface curvature and surface type features into binary feature codes. Li et al. [33] extracted and fused both the line and dominant direction features from the mean curvature images for 3D palmprint recognition. Similarly, Liu et al. [34] extracted the orthogonal line ordinal features from curvature-based images of 3D palmprint. In addition, the authors of [35] used the shape index image to represent the geometry feature of a 3D palmprint. Zhang et al. [36] formed a vector-based 3D palmprint descriptor by concatenating the block-wise surface type histograms and used the collaborative representation for feature identification. Bai et al. [37] developed a 3D palmprint recognition system by combining the block-wise surface type histogram descriptor and the principal component analysis (PCA). Cui et al. [38] proposed a 2D and 3D feature fusion method for 3D palmprint recognition by using two-phase test sample representation and PCA.

It is recognized that 3D palmprint images contain both the 2D texture-based and 3D surface structure-based features. How to exploit both the 2D and 3D features of 3D palmprint images will boost the accuracy of 3D palmprint recognition. In this paper, we exploit the visible and potential precision direction features for the 2D feature representation and use the compact surface type code to better represent the 3D surface features of a palmprint. Both the 2D-based precision direction and 3D-based compact surface type are combined to represent the multiple dimensional features of the palmprint for 3D palmprint identification. The contributions of this work can be summarized as follows:

- We exploit two precision direction features, including the visible and latent direction features of the palmprint, for the 2D feature representation of the 3D palmprint.
- We use a compact surface type code to represent the 3D surface structure features of the palmprint, which uses fewer codes to provide more efficient surface-based feature representation. The combination of precision direction and compact surface type can better represent the multiple level and multiple dimensional features of 3D palmprint images.

- We use a two-phase collaborative representation scheme to conduct the PDCST-based 3D palmprint identification. We conduct inter-comparisons between the proposed PDCST method and state-of-the-art 3D palmprint recognition methods and intra-comparisons among the different partials of the PDCST to demonstrate the effectiveness of the proposed method.

The rest of this paper is organized as follows. Section 2 prepares the related works for the proposed method of this paper. Section 3 proposes a multiple dimensional feature representation for 3D palmprint identification. Section 4 conducts the inter-comparative and intra-comparative experiments. Section 5 offers the conclusion of this paper.

2. Related works

In this section, we review the representative 2D direction feature extraction and representation of the palmprint, and prepare the curvature and surface type calculation methods of 3D palmprint images.

2.1. Direction features of palmprint

A palmprint contains rich discriminative line direction features, which can be exploited for palmprint recognition. The direction feature extraction of palmprint is based on one or multiple orientation-based templates. Specifically, a bank of templates with pre-selected orientations are defined, which are convolved with a palmprint and the convolved results are encoded into orientation feature codes. The orientation feature extraction of a palmprint can be represented as the following general formula:

$$\text{Orientation_feature_code}(x, y) = g(r) = g(T(\theta) * I(x, y)), \quad (1)$$

where $T(\theta)$ represents the template with orientation of θ , and I is an input palmprint image. “*” is the convolution operation. r denotes the convolved result between the template and palmprint. g is a mapping function converting the calculation result r into feature codes.

The competitive code method [21] is one of the most representative direction-based coding methods, which uses the real part of the Gabor filter as the direction-based template. That has the following form:

$$G(x, y, \theta, \mu, \sigma, \beta) = \frac{1}{2\pi\sigma\beta} \exp\left[-\pi\left(\frac{x'^2}{\sigma^2} + \frac{y'^2}{\beta^2}\right)\right] \cos(2\pi\mu x'), \quad (2)$$

where $x' = (x - x_0) \cos \theta + (y - y_0) \sin \theta$, $y' = -(x - x_0) \sin \theta + (y - y_0) \cos \theta$. (x_0, y_0) is the center of the function, μ is the radial frequency in radians per unit length, θ is the orientation of the Gabor filter in radians, and σ (β) is the standard deviations of the elliptical Gaussian along x (y) axis, respectively. The range of x and y are the sizes of the filter. The competitive code method uses six different directions of the Gabor templates to extract the dominant direction of the palmprint based on winner-take-all rule. Let $G(\theta_j)$ be the real part of the Gabor template with the direction of $\theta_j = j\pi/6$ ($j = 0, 1, \dots, 5$). The competitive code of a palmprint image is taken as:

$$\text{Competitive_code}(x, y) = \arg \min_j (r_j) = \arg \min_j (G(\theta_j) * I(x, y)), \quad \{j = 0, 1, \dots, 5\}. \quad (3)$$

The competitive code method is actually the direction of the Gabor template that achieves the largest filtering response with the palmprint. In addition, Luo et al. [16] proposed a dual competitive code method by extracting double direction codes with

the maximum and minimum filtering responses. In the template-based direction feature extraction, the templates are limited and their directions are discrete. It is possible that no template can better monitor the most dominant direction feature of palmprint. To extract more accurate direction feature, Xu et al. [39] improved the competitive code to the discriminative robust competitive code (DRCC) method. It argued that the accurate dominant direction usually located on the neighboring side of the competitive code with a larger filtering response than that of the other neighboring side. The DRCC of the palmprint can be extracted as follows:

$$DRCC_code = [O_c(x, y), O_s(x, y)] = \left[\arg \min_j (r_j), \text{sign}(r_{left(j)} - r_{right(j)}) \right], \quad (4)$$

where $\text{sign}(u)$ equals to 1 when $u \geq 0$, and 0 otherwise. $left(j)$ and $right(j)$ represent the two neighboring directions of the current dominant direction. Therefore, the DRCC, i.e. $[O_c, O_s]$, is the combination of the competitive code with a dominant direction side code.

The BOCV method [23] pointed out that using only one dominant direction feature to represent a local region may lose the information in the other direction. To this end, the BOCV method proposed to extract and encode multiple direction features of the palmprint. BOCV encode scheme can be represented as:

$$BOCV_code_i(x, y) = \text{sign}(T(\theta_i) * I(x, y)), \{i = 0, 1, \dots, 5\}. \quad (5)$$

The extended BOCV (E-BOCV) method [40] showed us that the BOCV codes with small convolved results are possibly the fragile bits, which should be marked by thresholding:

$$Fragile_code(x, y) = \text{sign}(|T(\theta) * I(x, y)| - \tau), \quad (6)$$

where τ is a positive thresholding parameter. The fragile code and stable BOCV code maps are respectively compared in the stage of palmprint matching. In addition, Sun et al. [28] extracted the multiple perpendicular direction features of the palmprint by using three combined orthogonal line Gaussian filters.

To improve the robustness of direction feature representation, the recent direction-based methods proposed to use the statistics of the selected direction features as the feature descriptor of the palmprint. For example, Luo et al. [41] formed the palmprint descriptor by concatenating the block-wise histograms of the two selected directions of the palmprint. In addition, Zhang et al. [28] used the block-wised histograms of the competitive code of the palmprint. Fei et al. [42] exploited the block-wise statistical features on the multiple dominant directions of the palmprint.

2.2. Curvatures and surface type of 3D palmprint

3D palmprint images depict the depth information of a palm surface with various convex and concave shapes. Given a point on a palm surface, it has multiple curvatures along different directions. Among them, the largest and smallest ones are considered as the most principal curvatures of the point. The mean value of these two principal curvatures is named as the mean curvature (MC) and the multiplication of them is called the Gaussian curvature (GC). Both the mean and Gaussian curvatures can depict the characteristics of a surface. In addition, the GC and MC shows high robustness to translation and rotation because they depend only on the surface shape but not on the way of the palm is placed in the 3D space. So the MC and GC are of two intrinsic measurements for 3D palmprint feature extraction and recognition.

It is hard to calculate all possible curvatures of a point on a surface to obtain its MC and GC. To address this issue, Besl et al. [43] provided us an effective way to obtain the MC and GC based on a group of pre-defined templates. In the following, we describe

Table 1
Nine surface type codes and corresponding surface shapes.

	GC > 0	GC = 0	GC < 0
MC < 0	Peak (STC = 1)	Ridge (STC = 2)	Saddle ridge (STC = 3)
MC = 0	None (STC = 4)	Flat (STC = 5)	Minimal surface (STC = 6)
MC > 0	Pit (STC = 7)	Valley (STC = 8)	Saddle valley (STC = 9)

the basic procedures of the mean curvature and Gaussian curvature calculations.

In general, a bank of partial derivative window templates are predefined as follows: $D_x = d_0 d_1^T$, $D_y = d_1 d_0^T$, $D_{xx} = d_0 d_2^T$, $D_{yy} = d_2 d_0^T$ and $D_{xy} = d_1 d_1^T$, where $d_0 = \frac{1}{7}[1\ 1\ 1\ 1\ 1\ 1\ 1]^T$, $d_1 = \frac{1}{28}[-3\ -2\ -1\ 0\ 1\ 2\ 3]^T$, $d_2 = \frac{1}{84}[5\ 0\ -3\ -4\ -3\ 0\ 5]^T$. Also, a binomial template is defined for smoothing 3D palmprint images: $S = ss^T$, where $s = \frac{1}{64}[1\ 6\ 15\ 20\ 15\ 6\ 1]^T$. Then, the partial derivative maps of a 3D palmprint f can be obtained as follows [36,43]:

$$f_u(x, y) = (D_u * (S * f(x, y))), \quad (u = x, y, xx, yy, xy). \quad (7)$$

Finally, the GC and MC can be directly obtained as:

$$MC = \frac{(1 + f_x^2)f_{yy} + (1 + f_y^2)f_{xx} - 2f_x f_y f_{xy}}{2(1 + f_x^2 + f_y^2)^{3/2}}, \quad (8)$$

and

$$GC = \frac{f_{xx}f_{yy} - f_{xy}^2}{(1 + f_x^2 + f_y^2)^2}. \quad (9)$$

To describe the characteristic of a 3D surface, Bsel et al. [43] classified a surface into eight fundamental types that is the surface type (ST). These STs depend on the signs and values of the MC and GC. It is pointed out that a special ST with $MC = 0$ and $GC > 0$ corresponding to non-existing surface shape is also used for completeness. As a result, nine surface types are used in representing the surface shape of 3D palmprint, which can be represented by using nine surface type codes (STC) as in Table 1. Therefore, the surface type of a point in 3D palmprint images can be represented as one of the nine STCs.

3. Precision direction and compact surface type representation

To extensively exploit the multiple dimensional features of 3D palmprint, we propose a precision direction code scheme to represent the 2D features and use a compact but efficient surface type code to represent the 3D features of the palmprint. Furthermore, we combine the precision direction with the compact surface type for more accurate 3D palmprint recognition.

3.1. Precision direction code

Existing works have proven that the dominant direction-based methods show promising performance in the direction-based method community. These methods are based on the observation that a palmprint contains many visible lines which generally carry dominant direction features. However, the visible lines are usually limited in a palmprint. Instead, plenty of points in a palmprint are in a flat area, carrying no visible direction feature.

The basic idea of direction feature extraction is based on a series of direction-based templates with multiple directions. Suppose that there are many templates with all possible directions used for the convolution of direction feature extraction. It is believed only a few templates, as well as the few directions, can obtain the maximum convolved response. Also, only a few directions of the templates can reach the minimum convolved response. Comparatively, a medium convolved response can be obtained by more templates

with more directions. Theoretically, the maximum and minimum convolved responses can only be achieved by a few directions of the templates. That means these directions have relatively higher discriminative power than other directions. A medium convolved response can possibly achieve by more directions. Thus, the corresponding directions possibly have low discriminative power. Therefore, one can assume that a point in a palmprint usually carry two potential direction features, including a normally visible direction feature and a latent direction feature. Inspired by this, we propose to extract more precision direction representation for both directions with the maximum and minimum convolved responses. Specifically, we convolve a palmprint image with pre-defined templates to obtain the convolved results as follows

$$c_j(x, y) = T(\theta_j) * I(x, y), \quad (10)$$

where $T(\theta_j)$ represent the direction-based template with direction of θ_j , and $\theta_j = (j - 1)\pi / N_\theta$. N_θ is the direction number of the employed templates. In this paper, we empirically use the Gabor filters as the templates and set the number of templates as: $N_\theta = 12$. Based on the convolved results, we can extract the first potential direction feature based on the maximum-based winner-take-all rule as follows:

$$DC_{\max}(x, y) = \arg \max_j (c_j(x, y)). \quad (11)$$

In real operations, the employed templates are usually limited and it is possible that no template has the same orientation as the dominant direction of the palmprint. In this case the extracted direction may not precisely represent the dominant direction feature of the palmprint. It is seen that a template with a more similar direction as the exact dominant direction of the palmprint generally can produce a larger response than the others. In other words, the more precision direction feature is generally on the neighboring side of the DC_{\max} with a larger convolved response than the other one. Inspired by this, we propose to extract a precision direction side code as follows:

$$SC_{\max}(x, y) = \text{sign}(c_{\text{mod}(DC_{\max}+1, N_\theta)}(x, y) - c_{\text{mod}(DC_{\max}-2+N_\theta, N_\theta)+1}(x, y)), \quad (12)$$

where “mod” is the modular operator. Intuitively, the side code can be used as a supplementary of the extracted dominant direction to precisely represent the direction feature of the palmprint. Similarly, we extract another potential direction feature from the minimum-based winner-take-all rule and the corresponding precision direction side code as follows:

$$DC_{\min}(x, y) = \arg \min_j (T(\theta_j) * I(x, y)), \quad (13)$$

and

$$SC_{\min}(x, y) = \text{sign}(c_{\text{mod}(DC_{\min}-2+N_\theta, N_\theta)+1}(x, y) - c_{\text{mod}(DC_{\min}+1, N_\theta)}(x, y)). \quad (14)$$

After that, we can obtain the precision direction code (PDC) of the palmprint image as follows:

$$PDC = [PDC_{\max}, PDC_{\min}] = [DC_{\max} \times 2 - SC_{\max}, DC_{\min} \times 2 - SC_{\min}]. \quad (15)$$

It is seen that PDC consists of two basic components, including the maximum-based precision direction and the minimum-based precision direction features, which correspond to the commonly visible and the potential invisible direction features of palmprint, respectively.

3.2. Compact surface type code

The conventional methods use nine codes to represent the surface types of 3D palmprint images based on the positive, negative

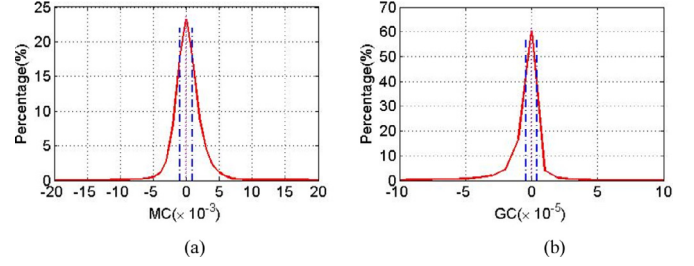


Fig. 1. The curvature distributions of 100 3D palmprint images. (a) The Mean curvature distribution; (b) The Gaussian curvature distribution.

signs and zero-values of the curvature features. In practical calculations, the mean and Gaussian curvatures of 3D palmprint images are floats. To determine the cases of $MC = 0$ and $GC = 0$, they normalize the curvatures falling into the range of -1 to 1 , and set the curvatures with small absolute values to zero.

3D palmprint images are usually captured with palms completely opened and flat, resulting a lot of small curvatures of the points. Fig. 1 depicts the mean curvature and Gaussian curvature distributions of 100 3D palmprint images randomly selected from the PolyU 3D palmprint database [44], showing that numerous points have small curvature values around zero. Therefore, the conventional methods use a very small threshold to define the range of the zero-curvature cases [32,36]. In other words, two small thresholds including a positive one and a negative one are actually used, as shown in Fig. 1.

It is believed that the curvatures of those points around the two thresholds are easily influenced by external noises, such as sweat, dirt, and the changes of the palm opening degree, and they are named as unreliable points. The curvature of an unreliable point may be encoded into a correct code or it may not. The curvature encodings are random events as the likelihood of curvature codes can be correctly encoded or not is equal. Therefore, we can assume that the number of error encoding points follows the Binomial distribution:

$$N_{err} \sim B(n, p), \quad (16)$$

where p is the error curvature encoded probability of an unreliable point and n denotes the total number of the unreliable points. The likelihood of the curvature encoding error (CEE) of a palmprint sample can be represented as:

$$\phi = 1 - (1 - p)^n. \quad (17)$$

It is seen that the likelihood of CEE completely relies on the number of unreliable points (n) and the error curvature encoded probability (p) of the unreliable points, where p is mainly determined by the palmprint images. Therefore, one can argue that the likelihood of CEE can be decreased by reducing n . We see that the conventional curvature encoding scheme based on the absolute value (abs-encoding) essentially use two small thresholds, including a positive threshold and a negative one. Intuitively, we can use a single zero threshold to encode, referred to as zero-encoding, the curvature features to reduce n . In the following, we show the likelihood of CEE in the zero-encoding scheme.

For the zero-encoding scheme, the unreliable points are generally referred to as the points whose curvatures are close to zero. We can reasonably assume that the number of error encoding points follows the Binomial distributions:

$$N_{err} \sim B(m, q), \quad (18)$$

where q is the error curvature encoded probability of an unreliable point and m is the total number of the unreliable points. The likelihood of CEE for the zero-encoding can be represented as:

$$\phi = 1 - (1 - q)^m. \quad (19)$$

Table 2

The compact surface type representation.

	GC > 0	GC < 0
MC > 0	CSTC = 1	CSTC = 2
MC < 0	CSTC = 3	CSTC = 4

For the zero-encoding scheme, the unreliable points are referred to the points whose curvatures are close to zero. Therefore, the total number of unreliable points is proportional to the percentage of the zero-curvature. In contrast, the unreliable points of the abs-encoding scheme are mainly the points whose curvatures are close to the positive and negative thresholds, both of which are very close to zero. It is not hard to deduce from Fig. 1 that the sum percentage of the unreliable points on the two non-zero thresholds is larger than the percentage of the zero value. Thus, the total number of unreliable points of the abs-encoding scheme (e.g. n) is larger than that (e.g. m) of the zero-encoding.

In general, the encoding error of the zero-encoding scheme is mainly created by the changes of concavity and the encoding error of abs-encoding scheme is easily affected by the degree of bending the palmprint surface. It is thought that a convex (concave) palm surface is difficult to change to a concave (convex) one. By contrast, the bending degree of the palm surface is easy to change with the opening degree of palms. Therefore, the error probability of zero-encoding scheme is possibly lower than that of the abs-encoding scheme, that is $q < p$. Therefore, the likelihood of the CEE in the abs-encoding scheme is possibly larger than that of the zero-encoding scheme. That is:

$$\phi_{abs-encoding} > \phi_{zero-encoding}, \quad (20)$$

which motivates us to use a simple zero threshold to encode the curvature features. Inspired by this, we propose to use a compact surface type (CST), which uses only four compact surface type code (CSTC) as shown in Table 2, to represent the surface features of 3D palmprint images. It can be seen that the CST only depends on the signs of the curvatures and thus it is suitable for the float-based curvature encoding.

In summary, ST is widely used to represent surface features of 3D palmprint images. However, statistical results show that the curvatures of numerous points in 3D palmprint images are very small float. The conventional ST defines two thresholds to divide the curvature features of 3D palmprint into three intervals so that they are encoded into three codes, which will produce more encoding errors than that of using a single zero threshold. In addition, there is no real surface with $MC = 0$ and $GC > 0$. To this end, we propose to use the simple yet effective CST, which encodes the curvature features into two intervals based on the signs of them, to represent the surface features of 3D palmprint images.

3.3. TPTSR-based PDCST identification

PDC and CST respectively depict the different level and different dimensional features of 3D palmprint images. We believe that combining the 2D feature-based PDC with 3D feature-based CST can better represent the multiple dimensional features of 3D palmprint. We record the combination of the PDC and CST as PDCST. For better representation and removing the small misalignment of 3D palmprint images, we use block-wise statistics to represent the local features of 3D palmprint. Specifically, PDCST consists of two precision direction codes and one compact surface type code. For each code map, we calculate the block-wise histograms and concentrate all block-wise histograms forming a vector-based descriptor for palmprint identification.

The two-phase test sample sparse representation (TPTSR) method [27,45] provides us an effective way to conduct pattern

recognition. TPTSR has the close-form solution and thus has high run efficiency. In addition, TPTSR can improve the performance over the CR-based method [46] by simply performing two steps of collaborative representation without heavily affecting the efficiency. To this end, in this paper, we adopt the TPTSR to perform PDCST-based palmprint identification. In the following, we first briefly review the basic idea of TPTSR and then present the TPTSR-based PDCST identification.

TPTSR consists of two steps of sparse representation. The first step of TPTSR is to represent a test sample as the linear combination of the training samples as follows:

$$y = a_1x_1 + a_2x_2 + \dots + a_nx_n = XA, \quad (21)$$

where y is the test sample, $a_i (i = 1, 2, \dots, n)$ is the weight coefficient, and $x_i (i = 1, 2, \dots, n)$ is the training sample. $A = [a_1 a_2 \dots a_n]^T$ and $X = [x_1 x_2 \dots x_n]$. Both x and y are column-based vectors, that is the PDCST-based descriptor in this paper. In general, A can be directly calculated as: $A = (X^T X + \lambda I)^{-1} X^T y$, where λ is a small positive constant and I is the identity matrix. After that, M training samples that produce the M largest representing contributions, i.e., $a_i x_i$, are selected to form the training set in the second step of TPTSR. Therefore, the test sample can be represented as:

$$y = b_1x_{i_1} + b_2x_{i_2} + \dots + b_Mx_{i_M} = X'B, \quad (22)$$

where B is the coefficient matrix, which can be similarly obtained as the calculation of A . Hence, the residual of the j th class can be calculated as:

$$r_j = \|y - (b_{j_1}x_{j_1} + b_{j_2}x_{j_2} + \dots + b_{j_{n_j}}x_{j_{n_j}})\|^2, \quad (23)$$

where $j_k (k = 1, 2, \dots, n_j)$ represents the sequence number of k th training sample from the j th class. Finally, test sample can be identified into the class that produces the smallest residual.

It can be seen that the TPTSR first forms a linear representation for a query sample and calculates the contributions of the training samples to the query sample. In general, a training sample making a large contribution to the query sample is more likely to be highly related to the query sample and thus taken as a competitive training sample. As a result, the TPTSR selects a group of training samples (e.g. M samples) with the largest M contributions to form the competitive training sample set. In the second step of TPTSR, it uses the competitive training samples to linearly represent the query sample to conduct the identification [45].

The PDCST descriptor consists of three feature vectors, including the PDC_{max}, PDC_{min} and CST feature-based vectors. In this paper, for each feature map, we conduct TPTSR to obtain the representation deviation of each class. Then, we fuse the representation deviations of all classes of the training samples on three kinds of feature maps, which are finally used for identification. The complete procedure of the PDCST based palmprint identification is described in Algorithm 1.

4. Experiments

In this section, we conduct both the inter-comparative and intra-comparative experiments on the widely used palmprint databases to test the proposed method.

4.1. 3D palmprint identification

In this paper, we use the public PolyU 3D (PolyU_3D) [44] palmprint database to conduct inter-comparative experiments among the proposed PDCST method and the state-of-the-art 3D palmprint recognition methods. The PolyU_3D database contains 8,000 3D palm surface depth data of the 3D palmprint images collected from 200 volunteers. An individual provided 20 samples for both the left and right palms. Thus, there are 400 palms

Table 3

The identification accuracies (average accuracy \pm standard deviation) of different methods on the PolyU_3D palmprint image database.

#k	MCI_comp	MCI_Ordinal	SII_Comp_LBP	MCI_GCI_ST	ST_CR	PDCST_NN	PDCST_TPTSR
1	87.16 \pm 0.70	83.12 \pm 1.08	81.74 \pm 0.90	80.99 \pm 2.50	90.51 \pm 1.43	95.85 \pm 0.73	97.04 \pm 0.34
2	94.90 \pm 2.36	93.09 \pm 3.70	91.46 \pm 3.03	92.09 \pm 3.08	95.10 \pm 1.44	98.65 \pm 0.93	99.23 \pm 0.61
3	96.86 \pm 1.68	93.86 \pm 3.15	95.19 \pm 3.01	95.06 \pm 2.09	97.83 \pm 1.01	99.30 \pm 0.60	99.69 \pm 0.33
4	98.75 \pm 0.18	97.95 \pm 0.51	96.48 \pm 1.45	97.50 \pm 0.55	98.36 \pm 0.52	99.60 \pm 0.61	99.86 \pm 0.05

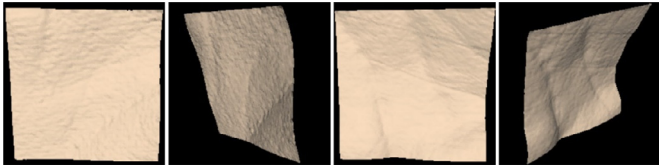


Fig. 2. Some typical 3D palmprint images of the PolyU_3D database. The first two images depict two different views of the same palmprint, and the other two images are from another palmprint.

of 3D palmprint image samples. In addition, the database includes the region of interest (ROI) of the 3D palmprint samples (128×128 pixels). Fig. 2 shows some typical 3D palmprint image samples of the PolyU_3D database. To the best of our knowledge, the PolyU_3D database is the most popular 3D palmprint image database typically used as the benchmark in the field.

Palmprint identification is the procedure of one-against-many comparisons to identify the class label of a query sample. Specifically, some labeled samples from each palm are selected as the training samples, and use the rest samples as the query samples. A query sample will be compared with training samples and identified based on the comparisons. In this paper, the proposed method identifies a query sample based on the representation residuals of the TPTSR. To evaluate the effectiveness of the TPTSR classifier, we use the conventional NN (Nearest Neighbor) scheme for the PDCST based identification and compare it with the TPTSR. Specifically, we calculate the Chi-square distance as the matching score of two PDCST-based descriptors and adopt the NN for identification. We write the proposed method with the TPTSR and NN classifiers as PDCST_TPTSR and PDCST_NN, respectively. In addition, the conventional state-of-the-art 3D palmprint recognition methods are also implemented and compared with the proposed method. The compared methods include the MCI-based competitive code method (referred to as MCI_Comp) [33], MCI-based ordinal code method (referred to as MCI_Ordinal) [34], the fusion method of SII based on competitive code and LBP features (referred to as SII_Comp_LBP) [35], the combination method of the MCI, GCI and ST binarization features (referred to as MCI_GCI_ST) [31], and the surface type-based collaborate representation method (ST_CR) [36].

In this study, we randomly select one to four samples ($k = 1, 2, 3, 4$) from each palm to form the training sample sets and use the remaining images as the query samples. We run each method 10 times, and report the average rank-one accuracy as well as the standard deviation on the four training sample sets. Table 3 summarizes the identification results of different methods, which shows that the proposed method consistently achieves higher accuracies than the five compared methods on the four training sample datasets. In addition, the TPTSR classifier outperforms the NN classifier, showing the effectiveness of the TPTSR in feature identification.

4.2. Effectiveness of the precision direction representation

The proposed PDCST method contains the 2D feature-based precision direction representation and the 3D feature-based CST representation. To validate the effectiveness of the precision direction representation, we conduct the 2D palmprint recognition experiment based on the PDC-based descriptor on the two-dimensional MCI palmprint image dataset recovered from 3D palmprint images (3D_MCI). Furthermore, two widely used 2D palmprint databases, including the PolyU 2D palmprint image database and the CASIA palmprint image database, are also used.

The PolyU 2D palmprint image database (PolyU_2D) [44] contains 7,752 palmprint 2D gray-level images collected from 193 different individuals, and each provided about 20 samples for both the left and right palms. The ROIs with the sizes of 128×128 pixels are also included in the database. The CASIA palmprint image database [47] claims that it contains 5502 2D palmprint images collected from 312 subjects. It is noted that the two subjects provided no sample and the last right palmprint image of the 270th subject does not belong to the individual. This means that the CASIA database includes 5501 2D palmprint image samples of 310 subjects with 620 palms, each of which has around 10 samples. In the experiments, the ROIs (128×128 pixels) of the palmprint images are cropped by the palmcode method [17].

Fig. 3 shows some palmprint examples selected from the 3D_MCI, PolyU_2D and CASIA palmprint datasets. It can be seen that different 2D palmprint images show different characteristics. PolyU_2D palmprint images are captured under a contact-based device and thus have better quality. The CASIA palmprint images are contactless palmprint images, which are captured under a free environment and show serious variant in translation and rotation. Both the PolyU_2D and CASIA palmprint samples show clearer texture features than that of the 3D_MCI. Therefore, we propose to use three different kinds of palmprint images to better test the PDC-based descriptor on 2D palmprint feature representation.

To evaluate the PDC-based method on 2D palmprint recognition, we compare it with state-of-the-art 2D palmprint recognition methods, including the competitive code method [21], ordinal code method [25], BOCV method [23], LLDP method [41] and the HOL method [26]. It is seen that the representative LLDP and HOL methods use the Chi-square distance to calculate the matching score of two compared palmprint samples. For a fair comparison, we use the Chi-square distance to compute the dissimilarity of two PDC-based descriptors. Similarly, we randomly select k ($k = 1, 2, 3, 4$) palmprint images from each palm as the training samples and treat the rest as the query samples for palmprint identification. Each method is repeated 10 times and the average accuracy is reported. Table 4 provides the comparative summary of the identification results, showing that the PDC based method consistently outperforms the five compared methods on all the training sample subsets.

Moreover, we conduct palmprint verification, which is a one-against-one matching procedure [11]. We calculate the false acceptance rate (FAR) and false rejection rate (FRR) for different methods and draw the ROC (FAR versus FRR) to compare different methods, as shown in Fig. 4. It illustrates that the PDC based method can

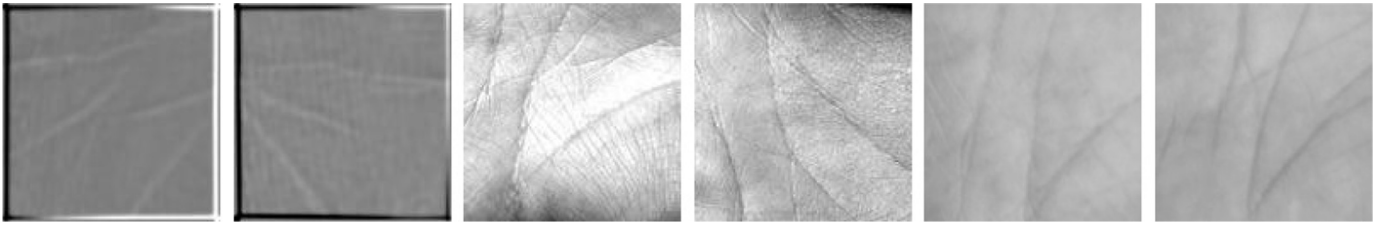


Fig. 3. Typical 2D palmprint samples selected from the 3D_MCI, PolyU_2D and CASIA palmprint datasets. The first two samples are from the 3D_MCI dataset; the middle two samples are from the PolyU_2D dataset; the last two samples are from the CASIA dataset.

Table 4
The rank-one identification accuracies of different methods on the 3D_MCI, PolyU_2D and CASIA palmprint image datasets.

	#k	Competitive	Ordinal	BOCV	LLDP	HOL	PDC
3D_MCI	1	90.39 ± 1.04	71.56 ± 1.54	77.83 ± 2.88	93.22 ± 0.85	87.871 ± 0.93	95.41 ± 0.77
	2	96.67 ± 2.36	84.30 ± 6.74	87.98 ± 3.88	96.33 ± 1.58	94.44 ± 2.98	98.67 ± 0.83
	3	97.84 ± 1.40	91.10 ± 1.73	93.89 ± 4.15	99.11 ± 0.16	96.84 ± 2.32	99.42 ± 0.43
	4	99.18 ± 0.12	92.23 ± 5.08	96.93 ± 0.25	99.46 ± 0.26	98.36 ± 0.52	99.48 ± 0.60
PolyU_2D	1	98.36 ± 0.15	93.15 ± 0.44	95.98 ± 0.24	99.04 ± 0.19	98.71 ± 0.77	99.53 ± 0.15
	2	99.81 ± 0.18	95.70 ± 0.64	98.12 ± 0.81	99.52 ± 0.26	99.61 ± 0.16	99.89 ± 0.08
	3	99.67 ± 0.29	97.34 ± 0.90	98.58 ± 0.99	99.73 ± 0.19	99.77 ± 0.15	99.90 ± 0.08
	4	99.85 ± 0.16	97.35 ± 0.94	98.23 ± 0.79	99.78 ± 0.17	99.78 ± 0.11	99.91 ± 0.06
CASIA	1	80.71 ± 1.84	72.48 ± 5.30	83.30 ± 1.41	87.34 ± 0.97	83.03 ± 0.47	87.43 ± 0.29
	2	88.60 ± 3.45	85.39 ± 5.22	91.10 ± 2.71	92.42 ± 1.90	88.37 ± 2.44	93.80 ± 1.18
	3	91.43 ± 3.18	87.31 ± 3.13	94.49 ± 0.05	95.08 ± 1.83	92.45 ± 2.88	95.23 ± 1.27
	4	92.64 ± 2.53	92.35 ± 1.10	94.39 ± 0.90	95.82 ± 1.21	94.87 ± 0.36	95.90 ± 0.59

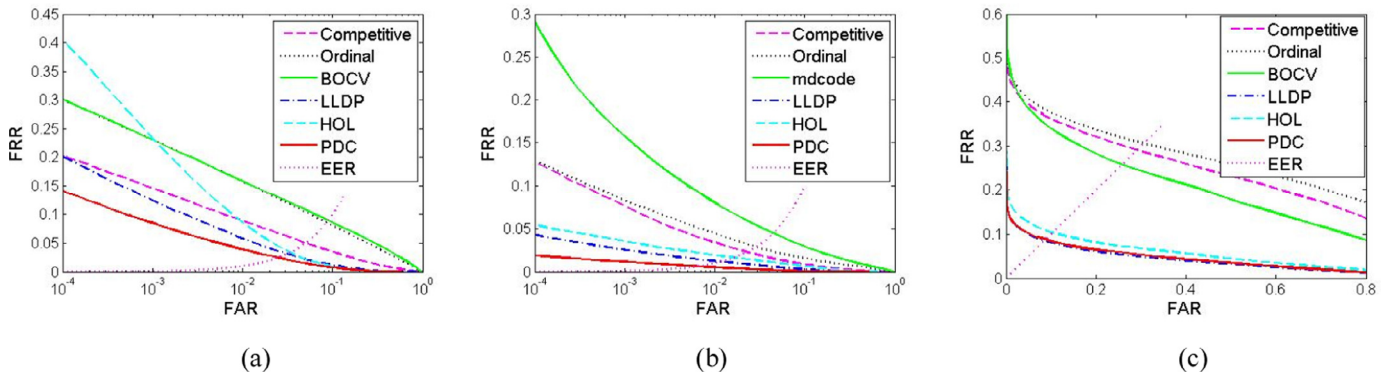


Fig. 4. The ROC curves of different methods. (a)–(c) The ROCs of six compared methods on the 3D_MCI, PolyU_2D and CASIA datasets, respectively.

achieve a lower EER than the five compared methods, demonstrating the effectiveness of the PDC on 2D palmprint representation.

4.3. Comparisons within PDC

The PDC consists of two components, that is, the precision direction code extracted based on the winner-take-all rule of the maximum convolved result, and the precision direction code extracted based on the winner-take-all rule of the minimum convolved result. Moreover, the precision direction code comprises a direction code and a side code. To further validate the effectiveness of PDC, we use the different components of the PDC as the feature descriptors for palmprint identification and verification. Specifically, we use the direction code extracted based on the maximum and minimum winner-take-all rules, which are recorded as DC_{max} and DC_{min}, respectively. Further, we use the precision direction codes, which is the combination of the direction code and the side code. Both precision direction codes based on maximum and minimum rules are recorded as PDC_{max} and PDC_{min}, respectively. For a fair comparison with the results of PDC, we obtain the feature descriptors by forming the block-wise based histograms of

Table 5
The rank-one accuracies of palmprint identification based on different feature descriptors on the 3D_MCI, PolyU_2D and CASIA palmprint image datasets.

	#k	PDC _{max}	DC _{max}	PDC _{min}	DC _{min}
3D_MCI	1	93.60 ± 0.58	92.20 ± 0.81	94.22 ± 0.67	93.86 ± 0.84
	2	97.42 ± 2.15	98.31 ± 1.00	97.28 ± 0.95	96.90 ± 1.34
	3	98.67 ± 1.08	98.51 ± 1.05	99.35 ± 0.14	99.07 ± 0.84
	4	99.12 ± 0.89	99.41 ± 0.20	99.49 ± 0.07	99.45 ± 0.11
PolyU_2D	1	99.58 ± 0.14	99.40 ± 0.22	99.30 ± 0.23	99.20 ± 0.27
	2	99.88 ± 0.05	99.81 ± 0.18	99.77 ± 0.13	99.72 ± 0.25
	3	99.92 ± 0.04	99.83 ± 0.16	99.76 ± 0.12	99.75 ± 0.12
	4	99.92 ± 0.08	99.89 ± 0.08	99.84 ± 0.16	99.80 ± 0.08
CASIA	1	84.81 ± 2.95	83.22 ± 2.92	84.14 ± 2.93	82.86 ± 2.82
	2	92.20 ± 2.18	90.01 ± 2.93	92.42 ± 1.67	91.72 ± 2.26
	3	94.02 ± 1.57	93.67 ± 1.66	93.68 ± 1.46	93.11 ± 2.19
	4	94.82 ± 1.26	93.88 ± 1.57	95.58 ± 0.70	93.41 ± 1.75

different code maps, and use the Chi-square distance for the comparison of different descriptors.

The procedures of palmprint identification and verification are similar as Section 4.2 and the results of them are shown in Table 5 and Fig. 5, respectively. It can be seen that the DC_{min} and PDC_{min} achieve comparable performances to DC_{max} and PDC_{max}, respec-

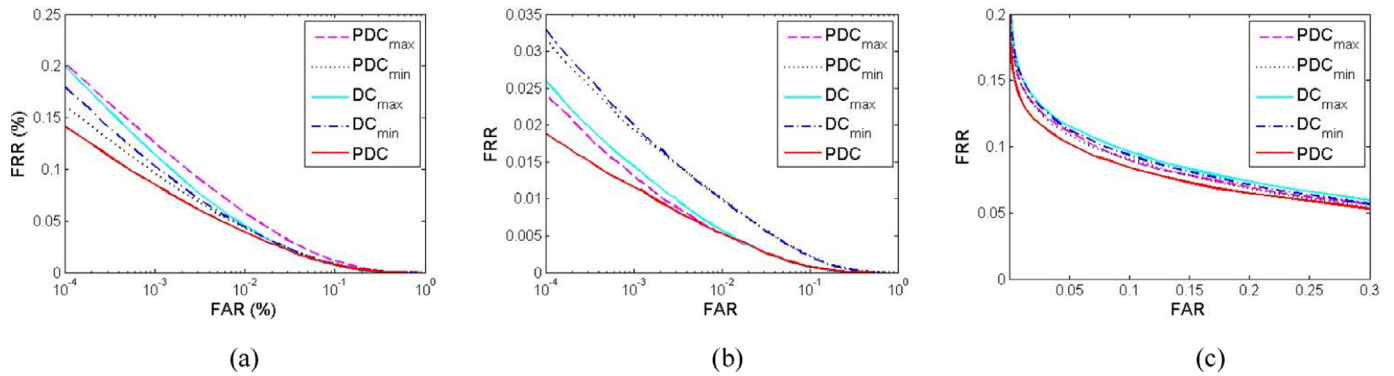


Fig. 5. The ROCs obtained based on different feature descriptors. (a)–(c) The ROCs of different feature descriptors on the 3D_MCI, PolyU_2D and CASIA datasets, respectively.

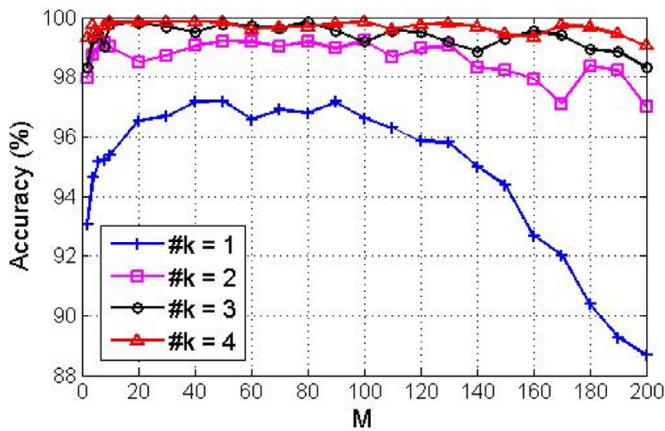


Fig. 6. The identification accuracies of TPTSR based palmprint identification with different M .

tively, demonstrating the comparable discriminative power of the potential invisible direction and the visible dominant direction features of the palmprint. Therefore, one can argue that the discriminability of the direction feature essentially depends on the winner-take-all rule but not on the maximum and minimum convolved results of the rule. In addition, both the PDC_{max} and PDC_{min} can achieve a comparable or better performance than the DC_{max} and DC_{min} , respectively, in most instances, showing the superiority of the precision direction over the conventional direction representation. Obviously, the PDC combining the PDC_{max} and PDC_{min} outperforms both of them.

4.4. Comparison between the ST and CST

To validate the effectiveness of CST, we conduct several comparisons between the ST-based and CST-based descriptors. We form the feature descriptors based on ST derived and CST derived block-wise histograms, and use the Chi-distance and TPTSR schemes to perform palmprint identification, respectively. We conduct palmprint identification by randomly selecting k ($k=1,2,3,4$) palmprint images for each palm as the training samples and the remaining as the test samples. Each method is performed 10 times and the average identification results are reported in Table 6. It is not hard to conclude that the CST-based descriptors consistently achieve better performances than the ST-based descriptors, which validates the effectiveness of CST in 3D surface feature representation of 3D palmprint images. This is true even through the conventional ST uses more surface type codes to describe a palm surface. However, it is hard to distinguish nine different surface types based on the curvature features of the palmprint because a plenty of points on

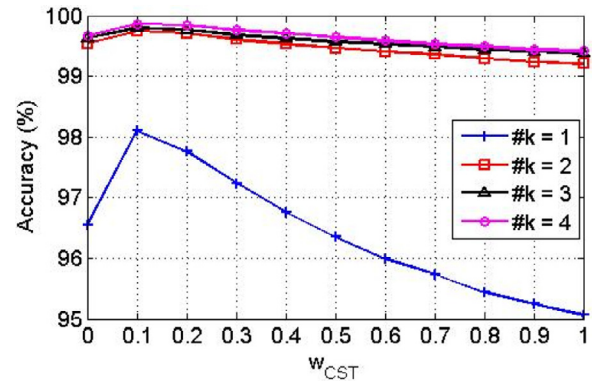


Fig. 7. The accuracy trend curve along w_{CST} .

Table 6

The rank-one identification accuracies obtained based on the ST-based and CST-based descriptors.

#k	ST-Chi	CST-Chi	ST-TPTSR	CST-TPTSR
1	88.28 + 1.12	89.12 + 1.00	92.69 + 0.67	94.92 + 0.52
2	94.00 + 2.19	95.04 + 3.05	94.83 + 1.37	98.41 + 1.60
3	97.26 + 2.21	97.88 + 1.56	99.21 + 0.04	99.59 + 0.08
4	98.68 + 0.26	99.35 + 0.06	99.52 + 0.11	99.65 + 0.23

the palmprint have very small curvatures. By contrast, CST provides us with a simple but effective way to represent the 3D surface features of 3D palmprint images.

4.5. M selection

The proposed method forms the PDCST-based 3D palmprint image descriptor and uses the TPTSR scheme for PDCST identification. The key step of TPTSR is to select M competitive training samples to represent a query sample. The selection of competitive training samples will affect the identification result of TPTSR, and a M value that is too large or small will reduce the identification accuracy. The CRC method [46] shows that it is the collaborative representation from all classes of training samples that improve the classification performance of sparse representation. In other words, it requires enough training samples to ensure the complete representation of the query sample. A small M means a few training samples are used, which possibly cannot guarantee the complete collaborative representation of the query sample, leading to a decline of the recognition performance. In addition, a large M will introduce some redundant and even noisy training samples to the representation of the query sample, resulting in the decreasing of identification accuracy. In addition, the optimal M values are possibly different for different query samples and different training samples.

Table 7

The computational time (s) of different methods in a palmprint identification procedure.

Methods	2-D feature extraction	3-D feature extraction	Identification
MCI_Comp	0.0107	0.0023	0.0243
SII_Comp_LBP	0.0193	0.0058	0.2359
MCI_GCI_ST	0.0014	0.0042	0.1696
PDCST_NN	0.0227	0.0040	0.0201
PDCST_TPTSR	0.0227	0.0040	0.0171

Algorithm 1

The procedure of the PDCST-based 3D palmprint identification.

Input: The training 3D palmprint images and a query palmprint image
Initialize: $M = 50$
For all the training samples and the query sample:
 1. Calculate the mean and curvature maps based on formulas (8) and (9);
 2. Calculate the PDC_{max} and PDC_{min} feature maps based on formula (15) and form the vector-based descriptors;
 3. Calculate the CST feature map based on Table 2 and form the vector-based descriptor;
End
 4. Form the three training feature matrices: X_i ($i = 1, 2, 3$) based on the PDC_{max} , PDC_{min} and CST feature maps of the training samples;
For each feature descriptor X_i ($i = 1, 2, 3$)
 5. Represent the query vector as Eq. (21) to select M competitive training samples;
 6. Represent the query vector as Eq. (22) based on the M competitive training samples;
 7. Calculate the residual (e.g. r_j^i) of j th class of training samples based on descriptor X_i by using Eq. (23);
End
 8. Fuse the residuals: $f_j = (r_j^1 + r_j^2 + r_j^3)/3$;
 9. The unknown sample is identified by the q th class, which produces the smallest residual: $q = \arg \min_i f_i$
Output: Identity of the query sample

To the best of our knowledge, there is no effective way to find the optimal M for different scenarios.

In this study, to show the effects of M on palmprint identification, we conduct TPTSR based palmprint identification by setting different M values. We randomly select different ($k = 1, 2, 3, 4$) palmprint images from each palm to form the training sample set and treat the rest as the test samples. We repeat the proposed method 5 times for each scenario and calculate the average identification accuracies, as shown in Fig. 6. It can be seen the optimal M values are different for different training sample sets, and they generally falls in the range of 10 to 100. A value of M that is too large or too small will result in obvious drops in identification accuracies. In addition, Fig. 6 shows that the identification accuracy is very close to the best one with a slight fluctuation when M falls in the range of from 10 to 100, which is consistent with the results of [45]. To this end, we empirically set M to an intermediate value, i.e. 50, in our manuscript.

4.6. Fusion of the multi-dimensional feature descriptors

The proposed PDCST method extracts two precision direction descriptors for 2D feature representation and one compact surface type descriptor for 3D feature representation of 3D palmprint images, and they are fused at the matching score level with equal weights. It is seen that both the PDC_{max} and PDC_{min} use 24 codes to depict the direction features, which are more than features of the CST. Therefore, the PDC_{max} and PDC_{min} should be more informative than the CST. To better show the affection of CST on the PDCST method, we test the performance of the proposed method with different weights for the PDC_{max} , PDC_{min} and

CST descriptors, referred to as $w_{PDC_{max}}$, $w_{PDC_{min}}$ and w_{CST} , respectively, and $w_{PDC_{max}} + w_{PDC_{min}} + w_{CST} = 1$. It is seen that the PDC_{max} and PDC_{min} have the similar coding schemes and thus we set $w_{PDC_{max}} = w_{PDC_{min}}$. Therefore, the fusion of the three descriptors in Algorithm 1 can be written as $f_j = \frac{(1-w_{CST})}{2} r_j^1 + \frac{(1-w_{CST})}{2} r_j^2 + w_{CST} r_j^3$.

We gradually increase w_{CST} from 0 to 1 with a step of 0.1, and conduct palmprint identification experiment, in which k ($k = 1, 2, 3, 4$) images from each palm are randomly selected as the training samples and the rest images are used as the query samples. For each case of w_{CST} and the training sample set, we repeat the proposed method 5 times and calculate the average identification accuracy, as shown in Fig. In addition, we draw the accuracy trend curve along w_{CST} , as shown in Fig. 7. It can be seen that the accuracy of the proposed method achieves the maximum on the point of $w_{CST} = 0.1$ and it gradually decreases with the increasing of w_{CST} , demonstrating the higher discriminability of the PDC_{max} and PDC_{min} over the CST. Even so, the fusion of the CST with the PDC can significantly improve the accuracy of 3D palmprint identification, showing the effectiveness of the CST. To our knowledge, there is no effective way to find the optimal weight combination. In this paper, we adopt the simple equal-weight fusion because the weight addition of the PDC_{max} and PDC_{min} is larger than that of the CST, and the accuracy of the equal-weight fusion is close to the best one.

4.7. Computational cost

The proposed method consists of multiple dimensional feature extraction and TPTSR-based identification. To better show the efficiency of the proposed method, we use the 3D_MCI samples calculate the computational time of the feature extraction as well as the feature identification, respectively. In addition, three baseline multiple-dimensional based methods, including the MCI_Comp, SII_Comp_LBP, and MCI_GCI_ST, are also implemented and compared with the proposed. To evaluate the efficiency of the TPTSR classifier, the PDCST descriptor with the NN classifier is also tested. For a fair comparison, all the methods are executed under the same platform containing a PC with an Intel(R) i7-7700CPU@3.60HZ, a 16 G RAM, and MATLAB R2014a. Each method is repeated 10 times and the average computational time, including the time taken for feature extraction and identification of a 3-D palmprint image, are reported in Table 7. It is pointed out that 2 samples for each palm are selected to form the training sample set and the time cost of curvature calculation is included in 3-D feature extraction. It can be seen that the proposed method takes a bit more time than the baseline competitive code methods in 2-D feature extraction. A possible reason is that the proposed method extracts twice the direction features as well as the extra corresponding side code information. By contrast, the proposed method has a relatively fast 3-D feature extraction speed due to the simple CST encoding scheme. In general, the feature extraction of the training samples can be performed outline before a query sample coming. Therefore, the efficiency of palmprint identification heavily

depends on the feature identification speed. It can be seen that the proposed method has the least identification time, making it suitable for palmprint identification. In addition, the TPTSR scheme of the proposed method is faster than the NN scheme, demonstrating the effectiveness of the TPTSR on palmprint identification.

5. Conclusion

A 3D palmprint image essentially contains both the 2D palmprint gray-level information and the 3D palm surface depth-level data. In this paper, we propose a precision direction descriptor to represent the 2D texture features and compact surface type to represent the 3D surface structure features for 3D palmprint recognition. The proposed precision direction code can better exploit both the visible and potential direction features of the palmprint. In addition, the conventional surface type is not very suitable to depict the surface features of 3D palmprint images because it is hard to distinguish nine surface types based on the small float-based curvature features of the palmprint. To solve this issue, we use a simple yet effective CST to represent the characteristics of a 3D palm surface. Furthermore, this paper combines the PDC and CST to form the PDCST, to provide more accurate 3D palmprint identification based on the two-phase sparse representation scheme. Extensive experimental results on three widely used palmprint databases have validated the promising performance of the proposed method on 3D palmprint identification as well as the effectiveness of the PDC and CST on feature representation of 3D palmprint. Hence, it would be interesting to exploit multiple precision directions to further improve the palmprint recognition performance, and to apply the CST to other 3D-based pattern recognition tasks to further demonstrate its effectiveness.

Acknowledgement

This work is partially supported by the National Key R&D Program of China under Grant No. 2018YFB1003201, the National Natural Science Foundation of China under Grant Nos. 61702110, 61673175 and 61602540, the Shenzhen Municipal Science and Technology Innovation Council under Grant No. JCYJ20170811155725434 and the Science and Technology Development Fund (FDCT) of Macau 124/2014/A3.

References

- [1] A.K. Jain, A. Ross, S. Prabhakar, An introduction to biometric recognition, *IEEE Trans. Circuits Syst. Video Technol.* 14 (1) (2004) 4–20.
- [2] D. Zhang, *Automated Biometrics: Technologies and Systems*, Springer Science & Business Media, 2013.
- [3] D. Zhang, *Advanced Pattern Recognition Technologies With Applications to Biometrics*, Medical Information Science Reference, 2009.
- [4] A.K. Jain, K. Nandakumar, A. Ross, 50 years of biometric research: accomplishments, challenges, and opportunities, *Pattern Recognit. Lett.* 79 (2016) 80–105.
- [5] D. Maltoni, D. Maio, A.K. Jain, S. Prabhakar, *Handbook of Fingerprint Recognition*, 2009.
- [6] X. Wang, X. Tang, A unified framework for subspace face recognition, *IEEE Trans. Pattern Anal. Mach. Intell.* 26 (9) (2004) 1222–1228.
- [7] F. Sun, Y. Yao, X. Li, L. Zhao, Type Curve Analysis of Superheated Steam Flow in Offshore Horizontal wells, *International Journal of Heat and Mass Transfer* 113 (2017) 850–860.
- [8] A. Kong, D. Zhang, M. Kamel, A survey of palmprint recognition, *Pattern Recognit.* 42 (7) (2009) 1408–1418.
- [9] L. Fei, G. Lu, W. Jia, S. Teng, D. Zhang, Feature extraction methods for palmprint recognition: a survey and evaluation, *IEEE Trans. Syst. Man Cybern.* (2018) 1–8.
- [10] A.K. Jain, J. Feng, Latent palmprint matching, *IEEE Trans. Pattern Anal. Mach. Intell.* 30 (6) (2009) 1032–1047.
- [11] D.S. Huang, W. Jia, D. Zhang, Palmprint verification based on principal lines, *Pattern Recognit.* 41 (4) (2008) 1316–1328.
- [12] W. Jia, B. Zhang, J. Lu, Y. Zhu, Y. Zhao, W. Zuo, H. Ling, Palmprint recognition based on complete direction representation, *IEEE Trans. Image Process.* 26 (9) (2017) 4483–4498.
- [13] D. Zhang, Z. Guo, G. Lu, L. Zhang, W. Zuo, An online system of multi-spectral palmprint verification, *IEEE Trans. Instrum. Meas.* 59 (2) (2010) 480–490.
- [14] Y. Xu, L. Fei, D. Zhang, Combining left and right palmprint image for more accurate personal identification, *IEEE Trans. Image Process.* 24 (2) (2015) 549–559.
- [15] D. Zhang, W. Zuo, F. Yue, A comparative study of palmprint recognition algorithms, *ACM Comput. Surv.* 44 (1) (2012) 1–37.
- [16] N. Luo, Z. Guo, G. Wu, C. Song, Joint Palmprint and Palmvein Verification by Dual Competitive Coding, in: *International Conference on Advanced Computer Control (ICACC)*, 2011, pp. 538–542.
- [17] D. Zhang, W.-K. Kong, J. You, L.M. Wong, Online palmprint identification, *IEEE Trans. Pattern Anal. Mach. Intell.* 25 (9) (2003) 1041–1050.
- [18] J. Dai, J. Zhou, Multifeature-based high-resolution palmprint recognition, *IEEE Trans. Pattern Anal. Mach. Intell.* 33 (5) (2011) 945–957.
- [19] X. Wu, D. Zhang, K. Wang, Palm line extraction and matching for personal authentication, *IEEE Trans. Syst. Man Cybern. Part A* 36 (5) (2006) 978–987.
- [20] W. Jia, D. Huang, D. Zhang, Palmprint verification based on robust line orientation code, *Pattern Recognit.* 41 (2008) 1504–1513.
- [21] A.W.K. Kong, D. Zhang, Competitive Coding Scheme for Palmprint Verification, in: *ICPR*, 2004, pp. 520–523.
- [22] A. Kong, D. Zhang, M. Kamel, Palmprint identification using feature-level fusion, *Pattern Recognit.* 39 (3) (2006) 478–487.
- [23] Z. Guo, D. Zhang, L. Zhang, W. Zuo, Palmprint verification using binary orientation co-occurrence vector, *Pattern Recognit. Lett.* 30 (2009) 1219–1227.
- [24] L. Fei, Y. Xu, W. Tang, D. Zhang, Double-orientation code and nonlinear matching scheme for palmprint recognition, *Pattern Recognit.* 49 (1) (2016) 89–101.
- [25] Z. Sun, T. Tan, Y. Wang, S. Li, Ordinal Palmprint Representation for Personal Identification, in: *CVPR*, 2005, pp. 279–284.
- [26] W. Jia, R.X. Hu, Y.K. Lei, Y. Zhao, J. Gui, Histogram of Oriented Lines for Palmprint Recognition, in: *IEEE Trans. Syst. Man Cybern.*, 44, 2014, pp. 385–395.
- [27] Z. Guo, G. Wu, Q. Chen, Palmprint recognition by a two-phase test sample sparse representation, in: *International Conference on Hand-Based Biometrics (ICHB)*, 2011, pp. 1–4.
- [28] L. Zhang, L. Li, A. Yang, Y. Shen, M. Yang, Towards contactless palmprint recognition: A novel device, a new benchmark, and a collaborative representation based identification approach, *Pattern Recognit.* 69 (2007) 199–212.
- [29] I. Rida, S. Maadeed, A. Mahmood, A. Bouridane, S. Bakshi, Palmprint identification using an ensemble of sparse representations, *IEEE Access* (6) (2018) 3241–3248.
- [30] J. Dai, J. Feng, J. Zhou, Robust and efficient ridge-based palmprint matching, *IEEE Trans. Pattern Anal. Mach. Intell.* 34 (8) (2012) 1618–1632.
- [31] D. Zhang, G. Lu, W. Li, L. Zhang, N. Luo, Palmprint recognition using 3-D information, *IEEE Trans. Syst. Man Cybern. Part C* 39 (5) (2009) 505–519.
- [32] D. Zhang, G. Lu, W. Li, L. Zhang, N. Luo, Three Dimensional Palmprint Recognition using Structured Light Imaging, in: *IEEE International Conference on Biometrics: Theory, Applications and Systems*, 2009, pp. 1–6.
- [33] W. Li, D. Zhang, L. Zhang, G. Lu, J. Yan, 3-D Palmprint recognition with joint line and orientation features, *IEEE Trans. Syst. Man Cybern. Part C* 41 (2) (2011) 274–279.
- [34] M. Liu, L. Li, Cross-correlation based Binary Image Registration for 3D Palmprint Recognition, in: *IEEE International Conference on Signal Processing (ICSP)*, 2012, pp. 1597–1600.
- [35] B. Yang, X. Wang, J. Yao, X. Yang, Efficient local representation for three-dimensional palmprint recognition, *J. Electron. Imaging* 22 (4) (2013) 043040–043040.
- [36] L. Zhang, Y. Shen, H. Li, J. Lu, 3D palmprint identification using block-wise features and collaborative representation, *IEEE Trans. Pattern Anal. Mach. Intell.* 37 (8) (2015) 1730–1736.
- [37] X. Bai, N. Gao, Z. Zhang, D. Zhang, 3D palmprint identification combining blocked ST and PCA, *Pattern Recognit. Lett.* 100 (2017) 89–95.
- [38] J. Cui, 2D and 3D palmprint fusion and recognition using PCA plus TPTSR method, *Neural Comput. Appl.* 24 (2014) 497–502.
- [39] Y. Xu, L. Fei, J. Wen, D. Zhang, Discriminative and robust competitive code for palmprint recognition, *IEEE Trans. Syst. Man Cybern.* 48 (2) (2018) 232–241.
- [40] L. Zhang, H. Li, J. Niu, Fragile bits in palmprint recognition, *IEEE Signal Process. Lett.* 19 (10) (2012) 663–666.
- [41] Y. Luo, L. Zhao, B. Zhang, W. Jia, F. Xue, J. Lu, Y. Zhu, B. Xu, Local line directional pattern for palmprint recognition, *Pattern Recognit.* 50 (2016) 26–44.
- [42] L. Fei, J. Wen, Z. Zhang, K. Yan, Z. Zhong, Local multiple directional pattern of Palmprint images, in: *ICPR*, 2016, pp. 3013–3018.
- [43] P. Besl, R.C. Jain, Segmentation through variable-order surface fitting, *IEEE Trans. Pattern Anal. Mach. Intell.* 10 (2) (1998) 167–192.
- [44] PolyU 2D and 3D Palmprint Databases, Available at: <http://www4.comp.polyu.edu.hk/~biometrics/>.
- [45] Y. Xu, D. Zhang, J. Yang, J.Y. Yang, A two-phase test sample sparse representation method for use with face recognition, *IEEE Trans. Circuits Syst. Video Technol.* 21 (9) (2011) 1255–1262.
- [46] L. Zhang, M. Yang, X. Feng, Sparse Representation or Collaborative Representation: Which Helps Face Recognition, in: *IEEE International Conference on Computer Vision (ICCV)*, 2011, pp. 471–478.
- [47] CASIA palmprint image database, <http://biometrics.idealtest.org/>.

Lunke Fei received the B.S. and M.S. degree from East China Jiaotong University, China, in 2004 and 2007, and received the Ph.D. degree in computer science and technology from Harbin Institute of Technology, China, in 2016. He is currently an associate professor with the School of Computer Science and Technology, Guangdong University of Technology, Guangzhou, China. His research interests include biometrics, pattern recognition, image processing and machine learning.

Bob Zhang received the B.A. degree in computer science from York University, Toronto, ON, Canada, in 2006, the M.A.Sc. degree in information systems security from Concordia University, Montreal, QC, Canada, in 2007, and the Ph.D. degree in electrical and computer engineering from the University of Waterloo, Waterloo, ON, Canada, in 2011. After graduating from Waterloo, he remained with the Center for Pattern Recognition and Machine Intelligence, and later was a Postdoctoral Researcher in the Department of Electrical and Computer Engineering, Carnegie Mellon University, Pittsburgh, PA, USA. He is currently an Assistant Professor in the Department of Computer and Information Science, University of Macau, Taipa, Macau. His research interests focus on biometrics, pattern recognition, and image processing. Dr. Zhang is a Technical Committee Member of the IEEE Systems, Man, and Cybernetics Society, an Associate Editor for the International Journal of Image and Graphics, as well as an Editorial Board member for the International Journal of INFORMATION.

Yong Xu received the B.S. and M.S. degrees in 1994 and 1997, respectively, and the Ph.D. degree in pattern recognition and intelligence system from the Nanjing University of Science and Technology, Nanjing, China, in 2005. Currently, he is with the Bio-Computing Research Center, Shenzhen Graduate School, Harbin Institute of Technology, Shenzhen, China. His current research interests include pattern recognition, biometrics, bioinformatics, machine learning, image processing, and video analysis.

Wei Jia received the B.Sc. degree in informatics from Central China Normal University, Wuhan, China, in 1998, the M.Sc. degree in computer science from Hefei University of Technology, Hefei, China, in 2004, and the Ph.D. degree in pattern recognition and intelligence system from University of Science and Technology of China, Hefei, China, in 2008. He has been a research assistant and associate professor in Hefei Institutes of Physical Science, Chinese Academy of Science from 2008 to 2016. He is currently a research associate professor in School of Computer and Information, Hefei University of Technology. His research interests include computer vision, biometrics, pattern recognition, image processing and machine learning.

Jie Wen received the M.S. degree at Harbin Engineering University, China in 2015. He is currently pursuing the Ph.D. degree in computer science and technology at Shenzhen Graduate School, Harbin Institute of Technology, Shenzhen, China. His research interests include, image and video processing, pattern recognition and machine learning.

Jigang Wu received the B.S degree from Lanzhou University in 1983, and the Ph.D. degree in computer software and theory with the University of Science & Technology China, Hefei, China, in 2000. He is currently a Professor with the Guangdong University of Technology, Guangzhou, China. He has authored 200 papers on computer magazines and international conferences. His current research interests include data science, computer network, machine intelligence, fault-tolerant computing.